

# Study of Reconstructed $^{39}\text{Ar}$ Beta Decays at the MicroBooNE Detector

The MicroBooNE Collaboration\*

June 28, 2018

In atmospheric argon,  $^{39}\text{Ar}$  beta decays occur at a rate of roughly one Becquerel per kilogram; as a result, large liquid argon time projection chambers (LArTPCs) see plentiful amounts of these decays in each event readout window. These  $^{39}\text{Ar}$  beta decays can provide a variety of different uses in LArTPC experiments. They allow for the study of reconstructing point-like ionization charge deposition in the detector, which is relevant for the reconstruction of supernova neutrino interactions. The point-like topology and well-known energy spectrum of  $^{39}\text{Ar}$  beta decays also provides a unique handle for calibrations. Presented here is the first study of reconstructing  $^{39}\text{Ar}$  beta decays in the MicroBooNE LArTPC. The spectrum of reconstructed electron energies from  $^{39}\text{Ar}$  beta decays, measured using raw TPC waveforms, is found to have a similar end point as the predicted distribution. Additionally, the signal shapes of reconstructed  $^{39}\text{Ar}$  beta decay candidates are used to validate the collection plane wire field response.

## 1 Introduction

Liquid argon time projection chambers (LArTPCs) can be used to reconstruct primary particles produced within the detector volume by detecting ionization signals at the anode wires, which detect ionization in a readout window that is several milliseconds in duration. Among other use cases (such as dark matter searches), these detectors are used to study the neutrino through its interaction with argon nuclei within the detector. This includes neutrinos produced in accelerators, with GeV-scale energies, as well as neutrinos of MeV-scale energies originating from stellar core-collapse supernovae. In order to understand the systematic uncertainties associated with reconstructing neutrinos of different energy scales, it is important to have a set of well-characterized ionization

---

\*microboone\_info@fnal.gov

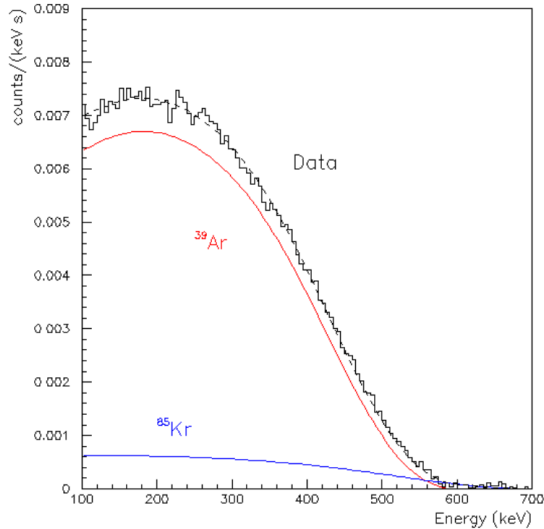


Figure 1: Illustration of the reconstructed energy spectrum of  $^{39}\text{Ar}$  beta decay electrons in the WARP liquid argon detector [1]. In this case, prompt scintillation light is used to reconstruct the energy of individual  $^{39}\text{Ar}$  beta decay electrons. Shown are fitted contributions from  $^{39}\text{Ar}$  and  $^{85}\text{Kr}$  after subtraction of other radiological background contributions. Note that the 6% energy resolution of the detector leads to a slight broadening of the spectrum.

sources in the detector that allow one to study reconstruction of particles of different energies in data. For MeV-scale supernova neutrino interactions, one candidate for these studies in LArTPC experiments is  $^{39}\text{Ar}$  beta decay, a low-energy radiological decay process with a cut-off energy of 565 keV; see Figure 1 for an example of the  $^{39}\text{Ar}$  beta decay electron energy spectrum as reconstructed by the WARP detector [1]. In atmospheric argon,  $^{39}\text{Ar}$  beta decays occur at a rate of roughly one Becquerel per kilogram [1]. As a result, large LArTPCs see plentiful amounts of these decays in each event readout window. These  $^{39}\text{Ar}$  beta decays allow for the study of reconstructing point-like ionization charge deposition in the detector, which is relevant for the reconstruction of supernova neutrino interactions. The point-like topology and well-known energy spectrum of  $^{39}\text{Ar}$  beta decays also allows for their use in a variety of different calibrations, as described below.

In order to obtain accurate energies, corrections must be made for charge attenuation and resolution that occurs due to various detector effects. LArTPC detectors operating on the surface, such as the one used by the Micro Booster Neutrino Experiment (MicroBooNE) [2, 3], are exposed to a large flux of cosmic rays with which to carry out calibrations of energy scale and resolution, using stopping cosmic muons as well as Michel electrons, neutral pions, and other cosmogenic activity. Underground LArTPC detectors, such as the ones that will be used for the far detector of the Deep Underground Neutrino Experiment (DUNE) [4, 5], will not have these large samples of cosmogenic

calibration sources. In each cubic meter of argon at the DUNE far detector (located roughly 1.5 km underground), approximately five cosmic rays will be observed each day, presenting a considerable challenge in calibrating out detector effects as both spatial and temporal precision in these measurements will be essential for reconstructing the energy of particles precisely and in an unbiased manner. One possibility is the use of  $^{39}\text{Ar}$  beta decay to enable various calibrations in large underground LArTPC detectors. The abundance of  $^{39}\text{Ar}$  beta decays in atmospheric argon provides a plentiful calibration source for detectors operating both on the surface and underground.

This work presents first studies of reconstructing  $^{39}\text{Ar}$  beta decays in the MicroBooNE LArTPC directed towards unlocking new calibration techniques for large LArTPC detectors. In addition, these studies demonstrate the viability of reconstructing point-like ionization deposition in large LArTPC detectors, which is relevant for the reconstruction of supernova neutrino interactions. First, LArTPC calibrations are discussed in Section 2, motivating the use of  $^{39}\text{Ar}$  beta decays in particular calibrations. Section 3 provides details of the selection of  $^{39}\text{Ar}$  beta decay candidates in data from the MicroBooNE TPC readout. In Section 4, the reconstructed  $^{39}\text{Ar}$  beta decay energy spectrum using MicroBooNE data events is presented and discussed in detail. The cosmogenic and radiological backgrounds to the  $^{39}\text{Ar}$  beta decay signal are discussed in Sections 5 and 6, respectively. In Section 7, a study of the shapes of the  $^{39}\text{Ar}$  beta decay signals as observed on the collection plane waveforms is discussed. Finally, conclusions and studies planned for the future are presented in Section 8.

## 2 LArTPC Calibrations

There are several detector effects that are relevant during the production of ionization electrons and their subsequent drift toward the anode wires. This includes space charge effects, or the modification of drift electric field in detector volume due to the build-up of slow-moving argon ions that are produced from e.g. cosmic rays. Another effect is charge quenching, characterized by the recombination factor,  $\mathcal{R}$ , which is the fraction of ionization charge that remains after prompt recombination with associated argon ions. Finally, there is the attachment of drifting ionization electrons to electronegative impurities such as oxygen and water in the argon, quantified by the electron lifetime,  $\tau$ . All of these effects must be precisely characterized in a LArTPC in order to make accurate and precise energy measurements. While space charge effects are relevant only for detectors operating on the surface, charge quenching and charge attenuation by attachment to impurities impact charge measurements in detectors operating both on the surface and underground. All three effects increase in magnitude as the drift electric field is lowered.

A number of calibration tools and systems are used or have been proposed to be used in LArTPCs, such as the use of cosmic ray muons, UV lasers, radioactive sources, and neutron sources.  $^{39}\text{Ar}$  beta decays offer a naturally available calibration source that does not require further technology installations. For LArTPC detectors operating on the surface, cosmic muons are typically used to perform a measurement of electron life-

time in the detector, as is done at MicroBooNE [6]; as discussed above, applying this approach in underground LArTPCs is complicated by low cosmic ray rates. Because the  $^{39}\text{Ar}$  beta decays are uniformly distributed in the drift direction, one is able to determine the expected reconstructed energy spectrum of  $^{39}\text{Ar}$  beta decays for a given set of detector response parameters. This can be done independently of using timing information (e.g. from prompt scintillation light), as it is not necessary to locate the position of any single  $^{39}\text{Ar}$  beta decay in the drift direction. The primary detector response parameters of interest are the electron lifetime and recombination factor; because these effects impact the shape of the energy spectrum differently, as shown in Figure 2, one can use the reconstructed  $^{39}\text{Ar}$  energy spectrum to measure these two quantities simultaneously. The impact of noise on the energy measurement will broaden these distributions, and so it is important for the noise level to be relatively small and precisely characterized; as discussed in Section 4, the effect is a smearing of roughly 60 keV at MicroBooNE, with data and simulation in good agreement.

Measuring effects of electron-ion recombination separately, at a greater precision than the measurement previously done at ArgoNeuT [7], would increase the sensitivity of an electron lifetime measurement using  $^{39}\text{Ar}$  beta decays. Other uses of  $^{39}\text{Ar}$  beta decays for calibrations in LArTPCs include diffusion measurements, measuring wire-to-wire response variations, and monitoring electric field distortions; some of these additional measurements, which make use of the beta decay signal shapes on TPC waveforms, are discussed in Section 7.

### 3 Beta Decay Candidate Selection

In the MicroBooNE TPC readout data,  $^{39}\text{Ar}$  beta decays look like points or very short “tracklets” that span fewer than 40 time ticks and less than four wires, where a time tick corresponds to roughly 0.56 mm in physical distance and the wire pitch is 3 mm at MicroBooNE (roughly 5 mm at the DUNE far detector). At a rate of about one Becquerel per kilogram, approximately 400 beta decays should be expected in each MicroBooNE TPC readout “event” (4.8 ms in duration). The individual  $^{39}\text{Ar}$  beta decays cannot be  $t_0$ -tagged, where  $t_0$  represents the time an individual decay occurred within the detector, because the prompt scintillation light from an individual decay is difficult to see in a large detector operating near the surface. This means that it is impossible to tell how far the ionization charge associated with an individual  $^{39}\text{Ar}$  decay has drifted in the TPC. However, this does not prevent an electron lifetime measurement in the detector as described above; the uniformity of the  $^{39}\text{Ar}$  beta decays in the drift direction would allow one to build the hypothesized energy spectrum associated with the decays for a given electron lifetime.

Specialized reconstruction techniques have been developed for small signals that use raw waveforms instead of the standard MicroBooNE reconstruction used for beam neutrino interactions and cosmics. The selection of  $^{39}\text{Ar}$  beta decays in MicroBooNE data, which is illustrated in Figure 3, utilizes the point-like properties of the beta decays. This measurement only uses the collection plane wires at present due to the higher

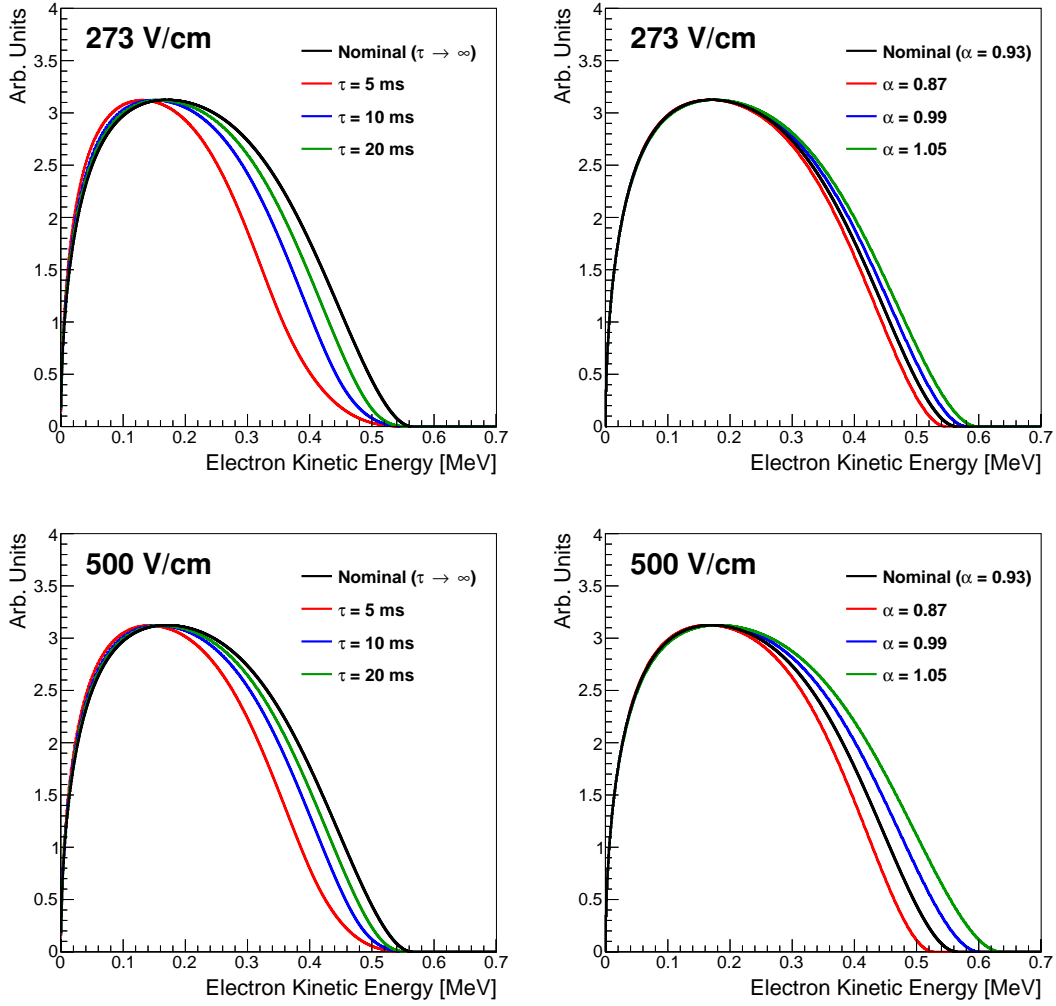


Figure 2: Illustration of the impact of different detector effects on the  $^{39}\text{Ar}$  beta decay electron energy spectrum for decays observed in the MicroBooNE detector at the nominal drift electric field of 273 V/cm (top row) and a drift electric field of 500 V/cm (bottom row). In the left column are examples of the energy spectrum for various different electron lifetimes, as well as the nominal  $^{39}\text{Ar}$  beta decay spectrum (corresponding to an infinite electron lifetime). In the right column are examples of the energy spectrum when the electron lifetime is infinite and the true recombination model is different from the one assumed in energy reconstruction (varying the  $\alpha$  parameter of the modified Box model,  $\mathcal{R} = \ln(\alpha + \xi)/\xi$ , where  $\xi = \beta \frac{dE}{dx} / \rho E_{\text{drift}}$ ,  $\rho$  is the density of the liquid argon, and  $\beta = 0.212 \text{ (kV/cm)(g/cm}^2\text{)/MeV}$  in this example). The nominal curve has been normalized to unit area, with the others scaled such that the peaks of the distributions line up.

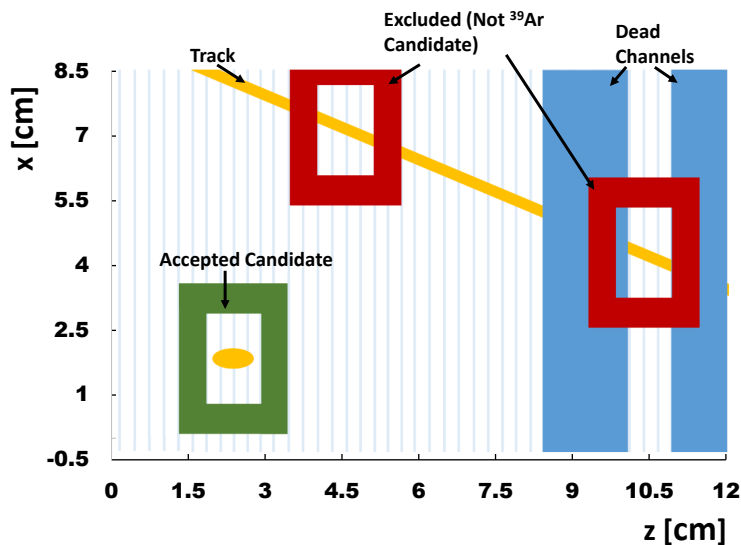


Figure 3: Illustration of  $^{39}\text{Ar}$  beta decay candidate selection method. The green and red boxes correspond to the check regions associated with specific points in the TPC readout window. The green box highlights an accepted  $^{39}\text{Ar}$  beta decay candidate, while the red boxes show cases when the selection method would reject the ionization activity contained within the check region boundaries (due to track-like activity overlapping with the window). Dead channels are also accounted for in this selection method.

signal-to-noise ratio of the collection plane in comparison to the two induction planes of the detector; this study will be extended to include the induction planes in the future. After the application of software noise filtering [8], the pedestal of each waveform is determined as the mode of the entire waveform and the pedestal-subtracted waveform is used forthwith. Then the collection plane event view is scanned wire by wire for points where charge exceeds a threshold, taken to be roughly five times the noise level in terms of equivalent noise charge (ENC) measured in number of electrons. At a threshold of  $1500 e^-$ , the contribution from large upward noise fluctuations to the number of reconstructed  $^{39}\text{Ar}$  beta decay candidates should be on the order of 1%, which is a negligible contribution for the present study. Note that this analysis is unique at MicroBooNE in the sense that all other analyses use advanced digital signal processing techniques (such as the deconvolution technique) [9,10] on the TPC waveforms before thresholding, whereas this analysis works directly with the raw TPC waveforms after noise filtering. This is possible because the collection plane wire field response is relatively simple (unipolar signal shapes) and so it is straightforward to threshold on the raw waveforms instead of requiring use of more sophisticated signal processing to condition the signals. Using the raw waveforms also allows for study of the wire field response directly using the  $^{39}\text{Ar}$  beta decay candidate signal shapes on the TPC waveforms, as is explored in Section 7.

After all charge over the specified threshold is located in the event readout, the event is scanned again, this time checking for signals that are consistent with a point-like topology. This is done by checking a small rectangular region around each point above threshold (the green and red boxes in Figure 3). The check region is nine wires by 80 time ticks, and has an inner region cut out so that true point-like activity does not veto itself. If there is charge above threshold found anywhere in the rectangular check region, due to an extended ionization track from a cosmic muon, for example, then the area is rejected. If the check region does not reject the point, then it becomes an  $^{39}\text{Ar}$  beta decay candidate. An integration window (of different size) is centered over the point of largest amplitude, and the charge within the region is integrated. The integration window is chosen to be three wires by 40 time ticks, which corresponds to 9 mm by 22 mm in physical distance; in the MicroBooNE coordinate system, the wire number increases in the  $z$  direction, while the time ticks increase in the  $x$  direction (the drift coordinate). These dimensions were chosen to be as small as possible while still containing the entirety of the  $^{39}\text{Ar}$  beta decay signal even in cases when the impact from diffusion in the detector is maximal (due to the charge drifting from near the cathode). An example of  $^{39}\text{Ar}$  beta decay identification in a single MicroBooNE TPC readout window is shown in Figure 4.

Steps are taken to actively mitigate the contribution of point-like activity associated with cosmics, such as photons or neutrons interacting in the argon, which are often located very close to the progenitor track. At the step where track-like activity is identified in the check region, a rough direction of the cosmic track is gathered based on where it intersects the rectangular check region. A flag is then set up in a region around the track to “veto” any nearby point-like activity that is potentially associated with the cosmogenic activity. Figure 4 illustrates the impact of the track veto on  $^{39}\text{Ar}$  beta decay reconstruction. The size of the “bubble” around the track is a single tunable parameter. The bubble is made of rectangles with a height (in time ticks) equal to six times the width (in number of wires), yielding approximately the same physical distance in both dimensions given the TPC readout digitization rate of 2 MHz and ionization drift velocity of 1.114 m/ms at a drift electric field of 273 V/cm. For the present study, a track veto window size of 20 cm is used. Any point-like activity found within these bubbles is excluded when building the reconstructed energy spectrum via the use of the aforementioned flag.

## 4 Reconstructed Energy Spectrum

In Figure 5, results of the  $^{39}\text{Ar}$  beta decay energy reconstruction are shown for the analysis of roughly one thousand MicroBooNE data events, recorded using random, non-beam triggers. Shown are the results of using two thresholds: a looser threshold optimized for MicroBooNE ( $1500\text{ e}^-$ ) and a tighter threshold to be used at the DUNE far detector ( $2200\text{ e}^-$ ) given the higher noise level associated with longer TPC wires [8]. The lower threshold of  $1500\text{ e}^-$  corresponds to roughly 100 keV of initial energy deposition (folding in the expected contribution from electron-ion recombination); for reference, the

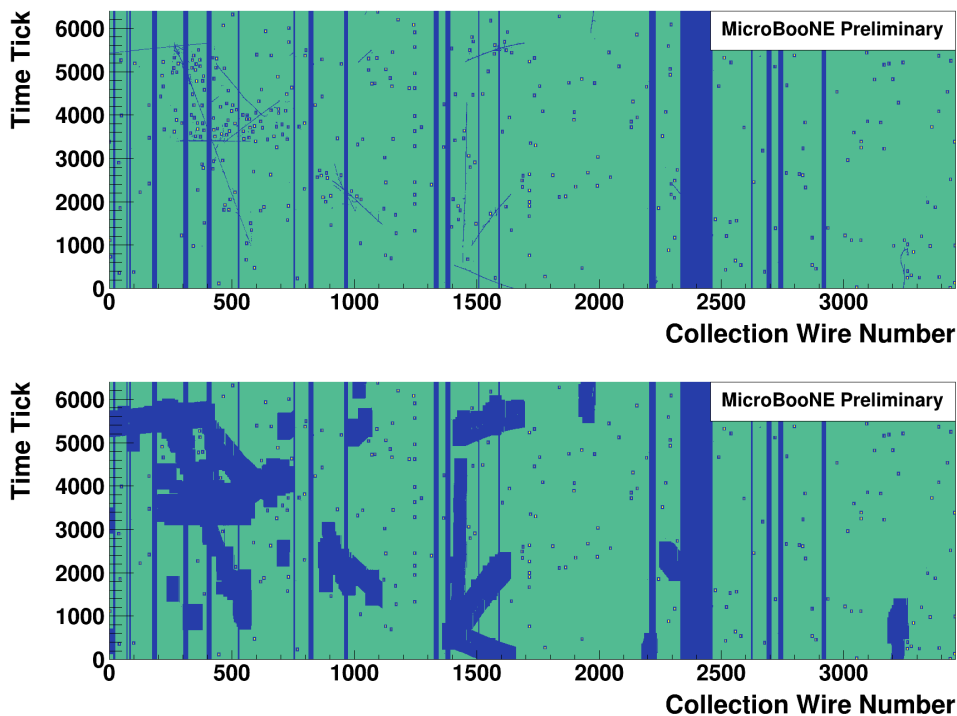


Figure 4: Collection plane event display showing the location of  $^{39}\text{Ar}$  beta decay candidates before (top) and after (bottom) the exclusion of regions near cosmic tracks. The narrow vertical bands are dead/noisy channels that are unusable in the analysis.

$^{39}\text{Ar}$  beta decay end point of 565 keV corresponds to nearly 12000  $e^-$  after recombination, while the MIP (minimum ionizing particle) energy scale corresponds to roughly 13000  $e^-$ . The  $^{39}\text{Ar}$  beta decay candidate energy is reconstructed by taking the charge in the integration window and applying a flat scale factor:

$$E = \frac{GI}{\mathcal{R}K} \times Q, \quad (1)$$

where  $E$  is the reconstructed beta electron kinetic energy in keV,  $Q$  is the measured charge in the integration window associated with the  $^{39}\text{Ar}$  beta decay candidate in units of  $\text{ADC} \cdot \text{ticks}$ ,  $G$  is the electronics gain in units of  $\text{electrons}/\text{ADC}$ ,  $I$  is the ionization energy in units of  $\text{keV}/\text{electron}$ ,  $\mathcal{R}$  is the average electron-ion recombination factor (unitless), and  $K$  is the signal area-to-amplitude factor that is associated with the measured TPC electronics response function in units of time ticks. Note that  $K$  is measured by taking the electronics shaping function of unit amplitude, with measured peaking time of approximately  $2.2 \mu\text{s}$  [10], and integrating the distribution after digitizing at 2 MHz (the sampling rate of MicroBooNE TPC waveforms). In the energy reconstruction, infinite electron lifetime is assumed; this is a reasonable approximation for the MicroBooNE

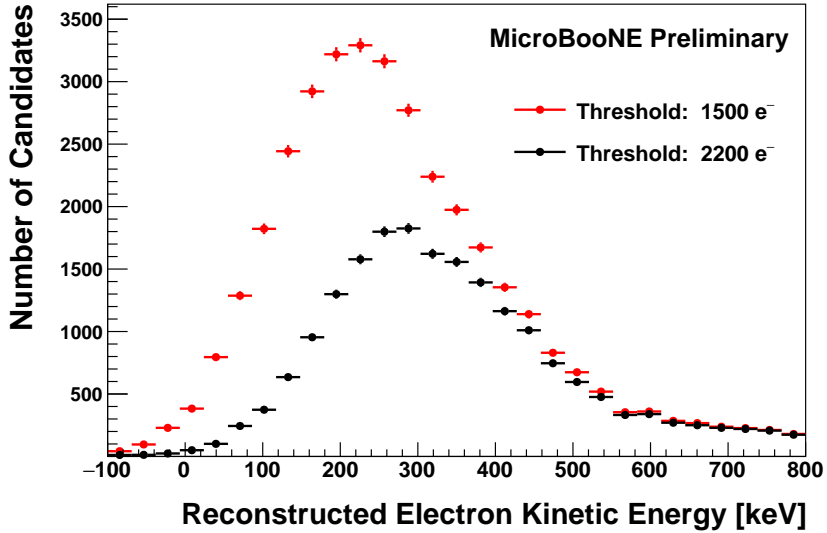


Figure 5: Reconstructed  $^{39}\text{Ar}$  candidate beta decay energy spectrum in MicroBooNE data for two different choices of threshold. Only the collection plane is used for the energy measurements, with infinite electron lifetime and  $\mathcal{R} = 0.5$  assumed. The looser threshold ( $1500\text{ e}^-$ ) corresponds to roughly five times the collection plane ENC (equivalent noise charge) at MicroBooNE, while the tighter threshold ( $2200\text{ e}^-$ ) corresponds to roughly five times the collection plane ENC that is expected in the DUNE far detector.

detector as the electron lifetime has been determined to be very high [6]. Estimated values for these last four quantities, which are constants in the energy reconstruction, are:  $G = 182$  electrons/ADC [8] (consistent with measurements using an external pulser [10]),  $I = 0.0236$  keV/electron,  $\mathcal{R} = 0.5$ , and  $K = 5.52$  ticks. Currently, space charge effects are ignored in the energy reconstruction, but they are expected to contribute modestly to energy reconstruction (less than 5% bias in reconstructed energy is expected) [11,12].

The reconstructed energy spectra shown in Figure 5 closely resemble the  $^{39}\text{Ar}$  beta decay spectra shown in Figure 2 with a few notable differences. First of all, there is a high-energy tail that is attributable to the presence of cosmogenic and radiological backgrounds in the selected sample. These backgrounds are discussed further in Sections 5 and 6, respectively. Additionally, the low-energy side of the spectra are sculpted due to effects of thresholding; the comparison of the two different thresholds used in Figure 5 clearly demonstrates the impact of thresholding on the energy reconstruction. Finally, the spectra are broadened due to the presence of noise in the integration window. The energy resolution associated with smearing due to the impact of noise is illustrated in Figure 6; for the chosen integration window of three wires by 40 time ticks, this corresponds to an energy resolution of roughly 60 keV (flat as a function of energy) for both data and Monte Carlo (MC) simulation.

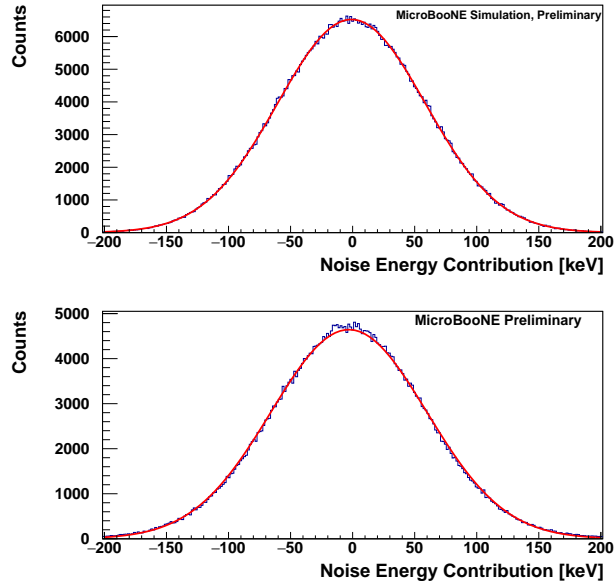


Figure 6: Study of energy resolution using randomly selected energy integration windows in MC (top) and data (bottom). The distributions are fit to Gaussian functions, yielding an energy resolution of 59 keV for MC and 63 keV for data.

Differences between data and simulation are still being understood, and so a direct comparison of the reconstructed  $^{39}\text{Ar}$  beta decay energy spectrum for data and simulation is not shown in this study. A comparison between data and simulation will be presented in a future work.

## 5 Cosmogenic Background

To better understand the contribution from cosmogenic sources to the high-energy tail of the reconstructed  $^{39}\text{Ar}$  beta decay energy spectrum, a Monte Carlo simulation making use of the CORSIKA event generator is studied. The reconstructed energy spectrum associated with this sample (roughly one thousand simulated TPC readout events) is shown in Figure 7. This distribution is found to fit a Crystal Ball function very well, which is also displayed in Figure 7. The Crystal Ball function is expressed as

$$f(x; \alpha, n, \bar{x}, \sigma) = N \cdot \begin{cases} \exp\left(-\frac{(x-\bar{x})^2}{2\sigma^2}\right) & \text{for } \frac{x-\bar{x}}{\sigma} > -\alpha \\ A \cdot \left(B - \frac{x-\bar{x}}{\sigma}\right)^{-n} & \text{for } \frac{x-\bar{x}}{\sigma} \leq -\alpha, \end{cases} \quad (2)$$

where

$$A = \left(\frac{n}{|\alpha|}\right)^n \cdot \exp\left(-\frac{|\alpha|^2}{2}\right), \quad (3)$$

$$B = \frac{n}{|\alpha|} - |\alpha|, \quad (4)$$

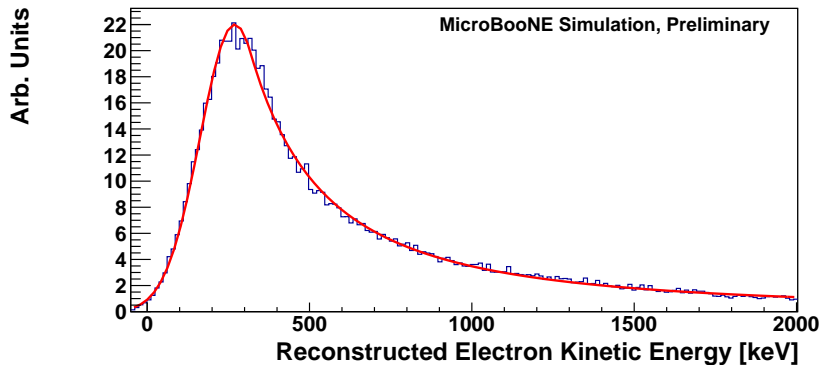


Figure 7: Result of fitting reconstructed energy distribution of cosmogenic background in MC to a Crystal Ball function.

$$N = \frac{1}{\sigma(C + D)}, \quad (5)$$

$$C = \frac{n}{|\alpha|} \cdot \frac{1}{n-1} \cdot \exp\left(-\frac{|\alpha|^2}{2}\right), \quad (6)$$

$$D = \sqrt{\frac{\pi}{2}} \left(1 + \operatorname{erf}\left(\frac{|\alpha|}{\sqrt{2}}\right)\right). \quad (7)$$

Given how well this function fits to a dedicated simulation of the cosmogenic background, one could use this in a multi-component fit to the data spectrum in order to separate out the contribution from cosmogenic backgrounds. However, the presence of higher-energy radiological backgrounds in the data sample complicates this somewhat, as discussed in the next section.

As mentioned in Section 3, the  $^{39}\text{Ar}$  beta decay candidate selection makes use of a track veto window around track-like activity detected in the TPC readout in order to remove the contribution from point-like cosmogenic activity. The reconstructed  $^{39}\text{Ar}$  beta decay energy spectrum is illustrated in Figure 8 for different choices of the track veto window size. No strong dependence of the reconstructed energy spectrum on the track veto window size is observed. Only a very minor shape difference is observed for data when looking at the normalized distributions. This is likely a result of the cosmogenic activity, which has a different spectral shape as observed in the CORSIKA Monte Carlo sample, being removed from the data sample.

## 6 Radiological Contamination

In addition to  $^{39}\text{Ar}$  beta decays, a number of other radiological contaminants are potentially contributing to the reconstructed energy spectra shown above. These radiological sources can either be distributed throughout the detector volume or localized to particular surfaces in the detector, such as the cathode or the field cage. A simulation

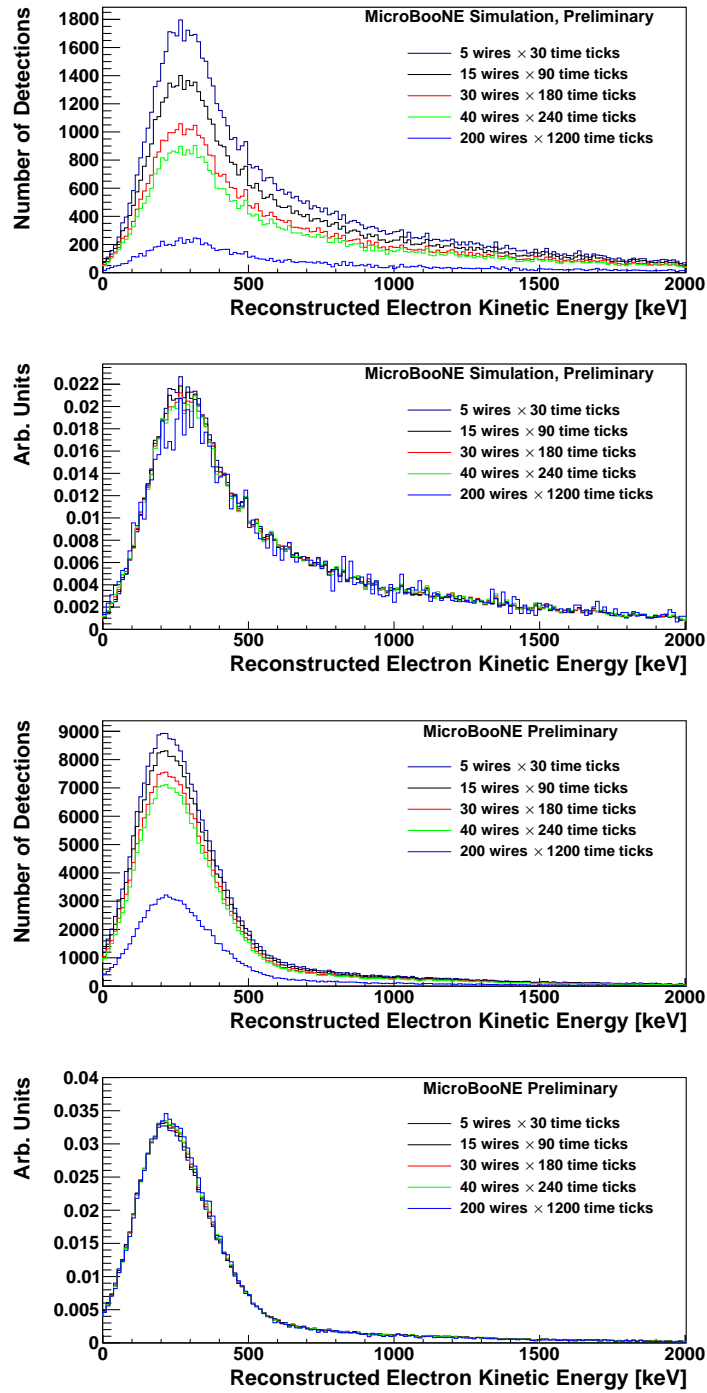


Figure 8: Comparison of reconstructed  $^{39}\text{Ar}$  beta decay energy spectra in a cosmic MC sample without simulation of any radiological decays (top two plots) and data (bottom two plots) for different choices of the track veto window. Shown are distributions before (top and third from top) and after (second from top and bottom) normalizing the curves to unit area.

was developed in order to study these potential radiological contaminants in more detail along side the  $^{39}\text{Ar}$  beta decays; the reconstructed energy spectra of a number of different radiological decays are shown in Figure 9.

Also illustrated in Figure 9 is a comparison of higher-energy radiological decays, namely the  $^{232}\text{Th}$  and  $^{238}\text{U}$  decay chains, to the background expected from cosmogenic activity in the detector. These decays can potentially explain part of the high-energy tail of the reconstructed  $^{39}\text{Ar}$  beta decay energy spectrum observed in data. However, given the similar spectral shape, it is difficult to separate out the component from cosmogenic activity and the component from the higher-energy radiological decays. This is a potential complication for a precise measurement of electron lifetime (or other detector parameters) using the reconstructed  $^{39}\text{Ar}$  beta decay energy spectrum in a LArTPC operating near the surface, such as MicroBooNE.

## 7 Signal Shape Study

In addition to measurements making use of the  $^{39}\text{Ar}$  beta decay energy spectrum, such as a measurement of electron lifetime, other detector parameters can be measured by utilizing the average signal shape of the beta decays in the TPC waveforms. Such measurements include a precise estimation of the diffusion constants (longitudinal and transverse) and wire-to-wire variations in the shape of the wire field response (due to deflection of some of the wires due to sagging, for instance), again folding in the knowledge that the  $^{39}\text{Ar}$  beta decays are uniformly distributed throughout the drift volume. The simple point-like topology of  $^{39}\text{Ar}$  beta decays makes it easier to perform these measurements as opposed to cosmic tracks, for instance. These measurements can be carried out in large LArTPC detectors as part of a more extensive calibration program without requiring the installation of any additional calibration hardware.

As a first investigation, the average waveform signal shape associated with  $^{39}\text{Ar}$  beta decays are studied in MicroBooNE data. Looking at the sample of one thousand readout events in data (corresponding to roughly 292,000  $^{39}\text{Ar}$  beta decay candidates), each reconstructed  $^{39}\text{Ar}$  beta decay is lined up in time and wire by the time tick and wire of highest amplitude. In this way, the “average signal shape” is reconstructed in two dimensions, averaging over both topology and drift-dependent effects such as diffusion. Figure 10 shows the two-dimensional average signal shape of  $^{39}\text{Ar}$  beta decay candidates in MicroBooNE data. This distribution can be compared to a simulation of  $^{39}\text{Ar}$  beta decays making use of various hypothesized diffusion coefficients in order to perform a measurement of the magnitude of diffusion; a measurement with MicroBooNE data is currently in development.

Also shown in Figure 10 are one-dimensional shapes associated with the three wires in the two-dimensional average signal shape. A shift of the average signal peaks on the side wires to earlier times, in comparison to the average signal shape on the central wire, is observed. This shift can be explained by the contribution of induced charge on the collection plane waveforms. While the majority of the signal on the collection plane is attributed to charge collection on the wire closest to the drifting ionization charge, there

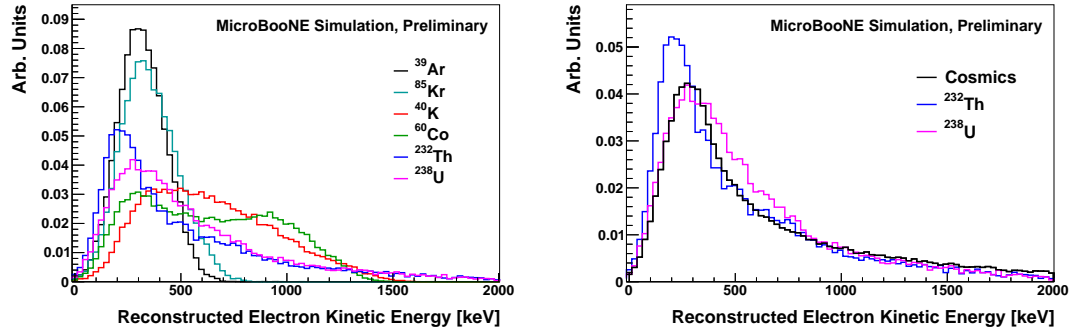


Figure 9: Reconstructed  $^{39}\text{Ar}$  candidate beta decay energy spectrum in simulation, comparing  $^{39}\text{Ar}$  signal to backgrounds from various radiological sources (left) and cosmogenic activity (right). On the right one can see that the contribution from cosmogenic activity is very similar to the  $^{232}\text{Th}$  and  $^{238}\text{U}$  decay chains.

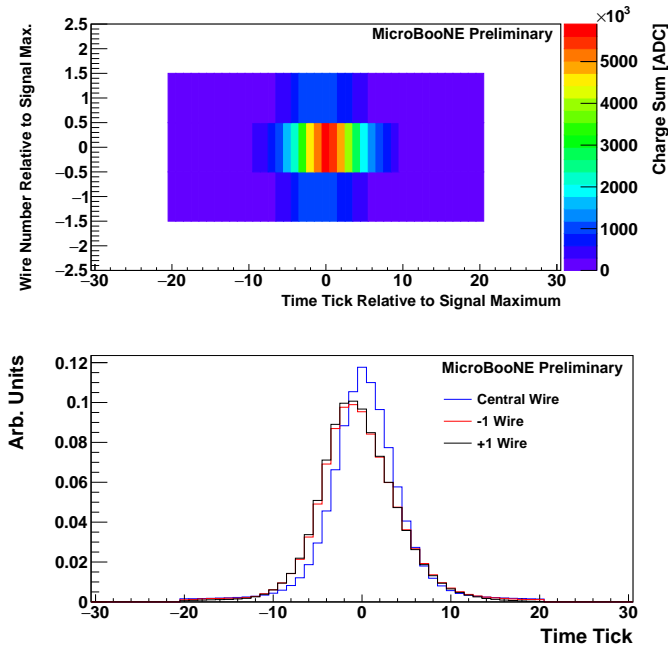


Figure 10: Average  $^{39}\text{Ar}$  beta decay signal shape as observed in waveform data. Shown are both a 2D view in time-wire space (top) and a 1D view in time for each of the three wires that contribute to signal reconstruction (bottom). While each distribution has been normalized to unity in the 1D view, note that the amplitude of the side wires are roughly 18% of the center wire amplitude.

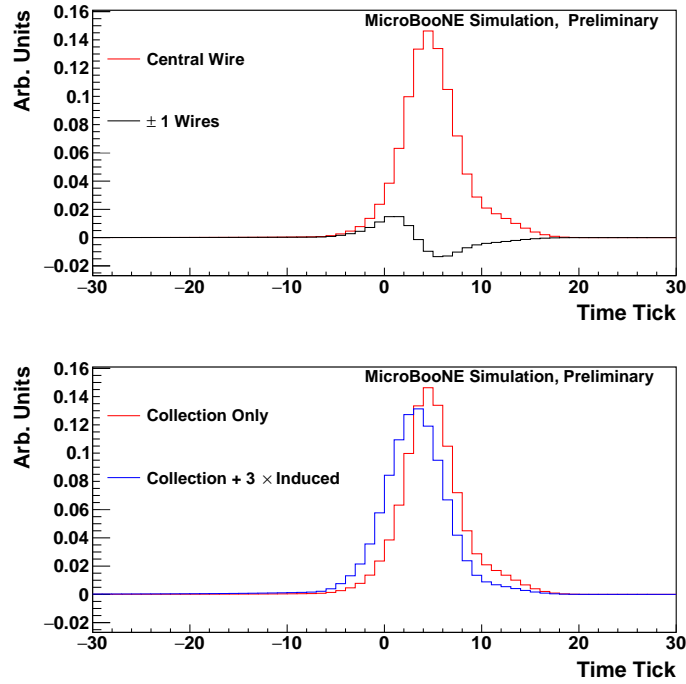


Figure 11: Illustration of the effects of induced charge on  $^{39}\text{Ar}$  beta decay reconstruction. On the top is a comparison of the nominal collection plane field response and the induced charge field response expected to be observed on the wires neighboring the charge-collection wire. On the bottom is the result of adding together these shapes; the blue curve is the sum of the red curve in the top plot and three times the black curve, normalized to unit area (this demonstrates the shape expected on the side wire if the central wire collects three times more charge than the side wire).

are also induction signals produced on neighboring wires that are smaller in magnitude. Figure 11 illustrates the relative size and shape of the collection signal on the central wire compared to the induction signal expected on adjacent wires as predicted by the Garfield simulation program. Note that these shapes are attributed to the wire field response only; Figure 10 includes contributions from electronics shaping and topological averaging, effects which primarily broaden these distributions. The positive and negative “lobes” of the induction signal, added together with the collection signal peak, can reproduce the shape observed in data that is shown in Figure 10; Figure 11 shows how adding a collection signal together with an induction signal associated with charge collected on a neighboring wire can replicate this shift. This study suggests that effects of induced charge play a non-negligible role even on the collection plane, and should be accounted for in signal processing of the TPC readout [9, 10].

## 8 Conclusions and Future Work

This work presents the first study of reconstructing  $^{39}\text{Ar}$  beta decays using ionization charge in a large LArTPC detector. The reconstructed energy spectra presented in Section 4 show not only that it is possible to reconstruct  $^{39}\text{Ar}$  beta decays in the MicroBooNE detector, but also that it should be possible to reconstruct this activity in the DUNE far detector with the noise level that is expected there. Being able to study reconstructed  $^{39}\text{Ar}$  beta decays in the DUNE far detector will be invaluable as it has the potential to provide an excellent and unique calibration source to pin down effects of electron lifetime, electron-ion recombination, diffusion, and wire-to-wire variation in field response. A more detailed study of the  $^{39}\text{Ar}$  beta decay spectrum in both MC and data as well as evaluation of the precision to which the MicroBooNE detector properties can be calibrated from the measured spectrum will be pursued in the near future. Complications due to cosmogenic backgrounds may ultimately limit the sensitivity of these measurements; the DUNE far detector, being located roughly 1.5 km underground, will not experience these complications.

In addition to performing measurements of detector parameters at MicroBooNE, other studies to extend the utility of  $^{39}\text{Ar}$  beta decays in LArTPCs are being planned. The reconstruction of  $^{39}\text{Ar}$  beta decays can be performed by combining information from the collection plane and the two induction planes in order to reconstruct the two-dimensional location of the  $^{39}\text{Ar}$  beta decays in the detector (the two dimensions orthogonal to the drift direction). In this way one would be able to make a measurement of electron lifetime as a function of these two dimensions, instead of the single dimension (in the beam direction) that the collection plane enables. This capability would be very useful at the DUNE far detector given the large size of the detector and the need to precisely determine the electron lifetime throughout the detector. Additionally, the study of  $^{39}\text{Ar}$  beta decays will lead to additional tuning of the simulation of lower-energy charge deposition in the detector. This tuning of the simulation will be invaluable for the study of supernova neutrino interactions in the DUNE far detector. Finally,  $^{39}\text{Ar}$  beta decay reconstruction will also be investigated at ProtoDUNE [13], the prototype detector for DUNE that will begin operations in August 2018.

## References

- [1] P. Benetti, “Measurement of the specific activity of Ar-39 in natural argon,” *Nucl. Instr. and Meth.A* 574, (2007) 83.
- [2] B. Fleming et al., “The MicroBooNE Technical Design Report,” *International Nuclear Information System* 48 (2014).
- [3] R. Acciarri et al., “Design and construction of the MicroBooNE detector,” *Journal of Instrumentation* 12, P02017 (2017).
- [4] R. Acciarri et al., “Long-Baseline Neutrino Facility (LBNF) and Deep Underground Neutrino Experiment (DUNE) Conceptual Design Report Volume 1: The LBNF and DUNE Projects,” *arXiv:1601.05471* [physics.ins-det] (2016).
- [5] R. Acciarri et al., “Long-Baseline Neutrino Facility (LBNF) and Deep Underground Neutrino Experiment (DUNE) Conceptual Design Report Volume 2: The Physics Program for DUNE at LBNF,” *arXiv:1512.06148* [physics.ins-det] (2016).
- [6] V. Meddage, “Electron attenuation measurement using cosmic ray muons in the MicroBooNE LArTPC,” *arXiv:1710.00396* [physics.ins-det] (2017).
- [7] R. Acciarri et al., “A study of electron recombination using highly ionizing particles in the ArgoNeuT Liquid Argon TPC,” *Journal of Instrumentation* 8, P08005 (2013).
- [8] R. Acciarri et al., “Noise Characterization and Filtering in the MicroBooNE Liquid Argon TPC,” *Journal of Instrumentation* 12, P08003 (2017).
- [9] C. Adams et al., “Ionization Electron Signal Processing in Single Phase LArTPCs I. Algorithm Description and Quantitative Evaluation with MicroBooNE Simulation,” Submitted to JINST, *arXiv:1802.08709* [physics.ins-det] (2018).
- [10] C. Adams et al., “Ionization Electron Signal Processing in Single Phase LArTPCs II. Data/Simulation Comparison and Performance in MicroBooNE,” Submitted to JINST, *arXiv:1804.02583* [physics.ins-det] (2018).
- [11] M. Mooney, “The MicroBooNE Experiment and the Impact of Space Charge Effects,” *arXiv:1511.01563* [physics.ins-det] (2015).
- [12] C. Adams et al., “Measurement of Space Charge Effects in MicroBooNE,” Publication in Preparation, <http://microboone.fnal.gov/public-notes/> (see MICROBOONE-NOTE-1018-PUB).
- [13] B. Abi et al., “The Single-Phase ProtoDUNE Technical Design Report,” *arXiv:1706.07081* [physics.ins-det] (2017).